Edge ambipolar potential in toroidal fusion plasmasa)

G. Spizzo, N. Vianello, R. B. White, S. S. Abdullaev, M. Agostini, R. Cavazzana, G. Ciaccio, M. E. Puiatti, P. Scarin, O. Schmitz, M. Spolaore, D. Terranova, and RFX and TEXTOR Teams

Citation: Physics of Plasmas (1994-present) **21**, 056102 (2014); doi: 10.1063/1.4872173
View online: http://dx.doi.org/10.1063/1.4872173
View Table of Contents: http://scitation.aip.org/content/aip/journal/pop/21/5?ver=pdfcov
Published by the AIP Publishing

Articles you may be interested in

Fluctuating zonal flows in the I-mode regime in Alcator C-Moda)
Phys. Plasmas **20**, 055904 (2013); 10.1063/1.4803914

Ohmic energy confinement saturation and core toroidal rotation reversal in Alcator C-Mod plasmasa)
Phys. Plasmas **19**, 056106 (2012); 10.1063/1.3695213

Three-dimensional effects on energetic particle confinement and stability a)
Phys. Plasmas **18**, 056109 (2011); 10.1063/1.3575626

Access to sustained high-beta with internal transport barrier and negative central magnetic shear in DIII-Da)
Phys. Plasmas **13**, 056110 (2006); 10.1063/1.2185010

Pellet fueling technology development leading to efficient fueling of ITER burning plasmasa)
Phys. Plasmas **12**, 056103 (2005); 10.1063/1.1865052

Re-register for Table of Content Alerts

Create a profile.

Sign up today!

This article is copyrighted as indicated in the article. Reuse of AIP content is subject to the terms at: http://scitation.aip.org/termsconditions. Downloaded to IP: 150.178.3.9 On: Tue, 06 May 2014 07:32:21

Edge ambipolar potential in toroidal fusion plasmas[a)]

G. Spizzo,[1,b),c)] N. Vianello,[1] R. B. White,[2] S. S. Abdullaev,[3] M. Agostini,[1] R. Cavazzana,[4] G. Ciaccio,[5] M. E. Puiatti,[1] P. Scarin,[1] O. Schmitz,[3] M. Spolaore,[1] D. Terranova,[1] and RFX and TEXTOR Teams

[1]*Consorzio RFX, Euratom-ENEA Association and Istituto Gas Ionizzati del CNR, Corso Stati Uniti, 4 35127 Padova, Italy*
[2]*Plasma Physics Laboratory, Princeton University, P.O. Box 451, Princeton, New Jersey 08543, USA*
[3]*Institut für Energieforschung-Plasmaphysik, Association EURATOM-FZJ, Jülich, Germany*
[4]*Consorzio RFX, Euratom-ENEA Association, Corso Stati Uniti, 4 35127 Padova, Italy*
[5]*Dipartimento di Fisica, Università degli studi di Padova, Padova, Italy*

(Received 22 November 2013; accepted 3 February 2014; published online 23 April 2014)

A series of issues with toroidally confined fusion plasmas are related to the generation of 3D flow patterns by means of edge magnetic islands, embedded in a chaotic field and interacting with the wall. These issues include the Greenwald limit in Tokamaks and reversed-field pinches, the collisionality window for ELM mitigation with the resonant magnetic perturbations (RMPs) in Tokamaks, and edge islands interacting with the bootstrap current in stellarators. Measurements of the 2D map of the edge electric field $E^r(r=a,\theta,\phi)$ in the RFX reversed-field pinch show that E^r has the same helicity of the magnetic islands generated by a m/n perturbation: in fact, defining the helical angle $u = m\theta - n\phi + \omega t$, maps show a sinusoidal dependence as a function of u, $E^r = \tilde{E}^r \sin u$. The associated E × B flow displays a huge convective cell with $v(a) \neq 0$ which, in RFX and near the Greenwald limit, determines a stagnation point for density and a reversal of the sign of E^r. From a theoretical point of view, the question is how a perturbed toroidal flux of symmetry m/n gives rise to an ambipolar potential $\Phi = \tilde{\Phi} \sin u$. On the basis of a model developed with the guiding center code ORBIT and applied to RFX and the TEXTOR tokamak, we will show that the presence of an m/n perturbation *in any kind of device* breaks the toroidal symmetry with a drift proportional to the gyroradius ρ, thus larger for ions ($\rho_i \gg \rho_e$). Immediately, an ambipolar potential arises to balance the drifts, with the same symmetry as the original perturbation. [http://dx.doi.org/10.1063/1.4872173]

I. INTRODUCTION

Magnetic islands in the plasma edge are either spontaneously present, due to the resonance with appropriate q values, or are produced by purpose with external coils, in order to stabilize pressure-driven modes which can be detrimental for confinement. In the first category fall the reversed-field pinch, characterized by the resonance of $m/n = 0/n$ modes at the $q = 0$ surface,[1] and the stellarator, with the resonance of small vacuum magnetic field errors with the Pfirsch-Schlüter current.[2] In the second category falls the tokamak, where the so-called resonant magnetic perturbations (RMP) have been successfully applied in DIII-D,[3] ASDEX,[4] and TEXTOR[5] to control edge-localized modes (ELMs) and/or spread the plasma-wall interaction on a larger surface. In this sense, the particle and power handling in ITER[6] is strictly linked to this type of studies.

A considerable effort has been devoted to the description of the topological features of the RMPs: especially in the German tokamak TEXTOR, detailed features of chaotic layers and islands has been thoroughly investigated.[7–9] Comparatively less studied are the kinetic effects on particles: the main result is that electrons respond quickly to magnetic chaos by increasing their diffusivity. Therefore, adding to a neoclassical base ion transport the effect of stochasticity, there is a development of a strong, positive radial electric field E^r to balance the enhanced electron diffusion.[10–12] This result for tokamaks echoes the studies of the electron and ion roots in stellarators, where $E^r > 0$ if the electron diffusion is larger than the ion's, $D_e \gg D_i$ (electron-root), and the converse, $E^r < 0$ if $D_e \ll D_i$ (ion-root).[13] But, apart from these general considerations, a detailed study of the electrostatic response to an edge magnetic island is still lacking. Generally speaking, electrons, ions, and impurities respond in quite a different way to magnetic islands: electrons follow more closely the magnetic field lines (and magnetic chaos), while ions drift away from the magnetic surface (larger gyroradius). The resulting electric field is determined by the ambipolar constraint: given a magnetic surface ψ, the fluxes must balance, $\Gamma_e(\psi) = \Gamma_i(\psi)$, and this prescribes the amplitude of the electric field (hence the name of "root" in stellarator studies). But the combination of $\vec{E}$ and the equilibrium $\vec{B}$ produces an $\vec{E} \times \vec{B}$ flow which can deeply affect transport on a macroscopic scale and mar plasma performance. In the RFX-mod reversed field pinch[14] (major radius $R = 2$ m, minor radius $a = 0.5$ m), there is a large body of evidence that the flow associated with the edge 0/1 island is ultimately responsible for an edge density peaking which drives the Greenwald limit.[15–17]

In this paper, we will describe an analytical model of the ambipolar potential response to an edge magnetic island,

[a)]Paper YI2 4, Bull. Am. Phys. Soc. **58**, 366 (2013).
[b)]Invited speaker.
[c)]Electronic address: gianluca.spizzo@igi.cnr.it

This article is copyrighted as indicated in the article. Reuse of AIP content is subject to the terms at: http://scitation.aip.org/termsconditions. Downloaded to IP: 150.178.3.9 On: Tue, 06 May 2014 07:32:21

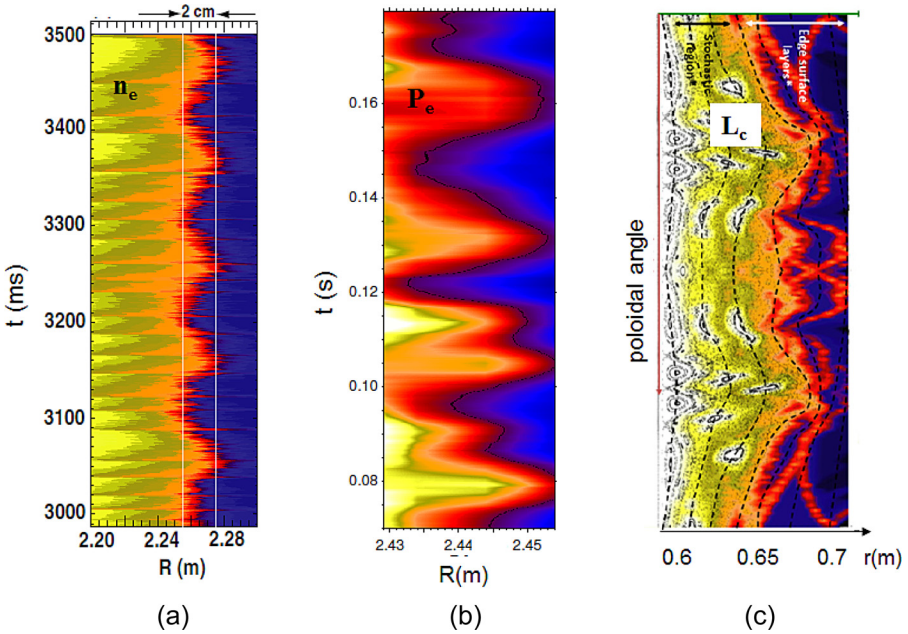

FIG. 1. (a) measurements of electron density profiles as a function of time (on y-axis) in the DIII-D Tokamak, while the 2/1 mode is rotating; (b) measurements of electron pressure profiles as a function of time, in the RFX-mod reversed field pinch, while the 1/7 mode is kept into slow rotation by the feedback system; (c) simulation of connection lengths L_c in the LHD stellarator, poloidal angle on the y-axis. In all of the three cases, radius is on the x-axis.

which has been introduced in test-particle simulations with the guiding-center code ORBIT.[18] The model for the potential satisfies the ambipolar condition $\Gamma_e = \Gamma_i$ on a magnetic flux surface close to the wall. Results are compared with data from RFX-mod and TEXTOR. The theory and data we present could be of interest for explaining the restriction for the collisionality window which characterizes ELM suppression with RMPs,[19] and the issue of the edge islands in stellarators.

The paper is organized as follows: Section II describes the main features of the measurements (mainly on the RFX-mod); Section III shows results of test-particle simulations with ORBIT, both in RFX and TEXTOR; Section IV shows how the model for the ambipolar potential works, and compares results with data from RFX and TEXTOR; finally, in Sec. V we draw our conclusions.

II. THE EXPERIMENTAL BASIS

It is often read in textbooks that the plasma edge is a smooth surface, symmetric along the toroidal angle ϕ. The name itself of "toroidal" confinement devices tacitly assumes the hypothesis that ϕ is a symmetry of the system. When measuring plasma kinetic properties, such as electron density or electron pressure, it is evident that reality is far from the idea of a smooth magnetic flux surface: in Fig. 1(a), electron density is plotted as a function of radius and time, while a 2/1 mode is made rotating with the I-coils in the lab frame of reference of DIII-D (the picture is adapted from Ref. 20). It is evident a modulation of density as a function of time, coherent with the phase of the magnetic mode. In Fig. 1(b), the same exercise is done in the case of electron pressure, when a 1/7 mode is kept slowly rotating by the feedback system[21] of the RFX-mod reversed-field pinch: again, electron pressure is modulated in time, while the mode is sweeping in front of the diagnostic (the picture is taken from Ref. 22). Finally, Fig. 1(c) shows a simulation of connection length (the parallel path along a field line from a given point to the wall), as a function of radius R and poloidal angle θ in the LHD stellarator: the surface is not smooth, and all kind of structures (ergodic "fingers," conserved regions, and laminar zones directly connected to the wall) are visible (the picture is adapted from Ref. 23). Considered globally, Fig. 1 shows that, despite formidable differences in the equilibrium fields, nature of transport, size of the device, type of input power, all of the three main magnetic confinement configurations, when confronted with 3D fields and magnetic chaos in the edge, show coherent and macroscopic modulations of kinetic quantities which can be easily put into relationship with the symmetry of the dominant magnetic island.

To explore this in more detail, we focus on one of the three configurations, namely the reversed-field pinch. Fig. 2 is the starting point for the studies on flow and islands in the edge: it shows the measurement of the toroidal component of plasma flow, v_ϕ, as a function of the helical angle u, in the case of a 0/1 island in the RFX-mod reversed field pinch. It is worth recalling that the equilibrium magnetic field in the edge of a reversed field pinch is *poloidal*, so that (v_r, v_ϕ) are the components of the *perpendicular flow*. The flow is measured by a gas-puff imaging diagnostic (GPI),[24,25] at a single point toroidally and at a radius $r = 0.98a$. Since the island is slowly rotating in the lab frame of reference, to map the measurement (which is a function of time) on the topology of the island, we use the definition of helical angle $u(\theta, \phi; t) = m\theta - n\phi + \omega_{m,n}t$, which in the case of a 0/1 island simplifies to $u_{0,1} = -\phi + \omega_{0,1}t$. One can interpret $u_{0,1}$ as the toroidal angle in a frame of reference rotating together with the island. Formally, it can be shown that the formula for $u_{m,n}$ is obtained quite naturally by expressing the Hamiltonian of field lines in action-angle variables:[26] in this way, any island that develops at a given m/n resonance has a similar shape, when plotted on the plane (u, ψ), with ψ the magnetic flux coordinate (for more details about the definition and use of the helical angle, the reader can refer to Ref. 22). The flow is generally negative over the helical angle, which would correspond to $E^r < 0$ (the diamagnetic term

This article is copyrighted as indicated in the article. Reuse of AIP content is subject to the terms at: http://scitation.aip.org/termsconditions. Downloaded to IP: 150.178.3.9 On: Tue, 06 May 2014 07:32:21

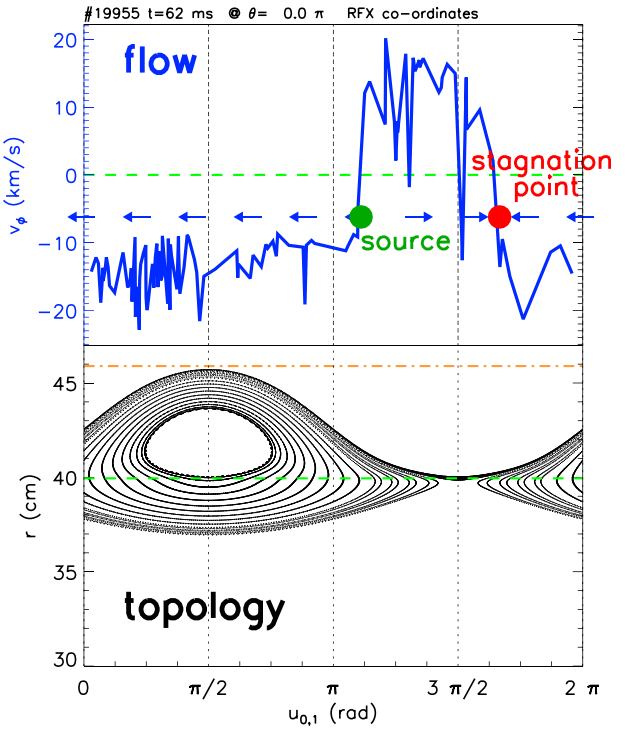

FIG. 2. (Top) Toroidal component of plasma flow, as a function of the helical angle $u_{0,1}$ and (bottom) corresponding 0/1 island, with the minor radius on the y-axis. The zeroes of the flow are marked as bullets, and correspond to a source and stagnation point for plasma density (green and red, respectively, in the online version of the figure).

accounts for at most 15% of the flow in RFX, so $E^r \approx v_\phi B_\theta$): this is the usual situation in RFX [see, e.g., Figs. 7(c) and 7(d) in Ref. 17], and has been interpreted in the past in terms of finite ion Larmor radius effects.[27] But there is a large portion of the toroidal angle where $v_\phi > 0$ ($E^r > 0$), with two null points that define a huge convective cell (diameter ~ 3 m). Looking at the arrows in Fig. 2, it is easy to recognize a "source" and a "stagnation" point. Recent measurements of the radial component of the velocity, v_r, confirm the presence of a convective cell, though in presence of a 1/7 island, instead than a 0/1:[28] during the year 2014, it is planned to measure v_r with a rotating 0/1 island, too. Actually, measurements showing that E^r could change sign in RFX along ϕ are not really new, dating back to more than ten years ago.[29,30] What is new is the interpretation in terms of magnetic islands in the edge: in fact, the *center of the convective cell corresponds to the X-point* (XP) of the 0/1 island, which is plotted in Fig. 2, bottom panel, while the O-point (OP) corresponds to the baseline $E^r < 0$. Namely, the flow possesses the same symmetry as the magnetic island. Finally, it is worth underlining that the convective cell can drive macroscopic changes in transport, such as toroidally localized edge density accumulation and radiation condensation, known in the Tokamak community as MARFE,[31,32] which is a precursor of the Greenwald limit. In fact, by increasing average density, the 0/1 island width increases, and at the same time magnetic chaos develops in the core, deteriorating global confinement and increasing influxes and, generally speaking, plasma-wall interaction.[33] It is also observed the formation of a very dense and cold annulus in the plasma edge, corresponding to enhanced radiation. This annulus is localized toroidally in $u_{0,1}$: in measurements, it is visible as a time-dependent, large density modulation in phase with the 0/1 mode, analogous to what seen in Fig. 1(b) for the 1/7 mode. It is also poloidally symmetric, which makes it in all respect similar to the tokamak MARFE (i.e., it is aligned along the edge equilibrium $\vec{B}$ field). In the RFX, evidence of a causal connection between the convective cell and the MARFE (and thus, the Greenwald limit) is compelling.[15–17]

To better understand the topology of the E^r field, we can map the measured values (as a function of u) onto an edge flux surface calculated with VMEC/V3FIT: the adaptation of VMEC to the reversed field pinch is a recent addition in the framework of a collaboration between Consorzio RFX and the Auburn University.[34] The result is shown in Fig. 3(a): in the colormap, blue corresponds to the potential well ($E^r > 0$ at $r = a$) while red corresponds to the potential hill ($E^r < 0$ at $r = a$). Axes (X, Y, Z) show the cartesian system, where the helical $u_{0,1}$ has been substituted for the usual toroidal angle ϕ. The potential well corresponds to the XP of the island, which, in terms of flux surfaces, is the region where the annulus is shrunk: thus, the symmetry of E^r is the same as the magnetic island. A nice proof that this is a general property has been obtained recently with the complete toroidal array of Langmuir probes, called ISIS (Integrated System of

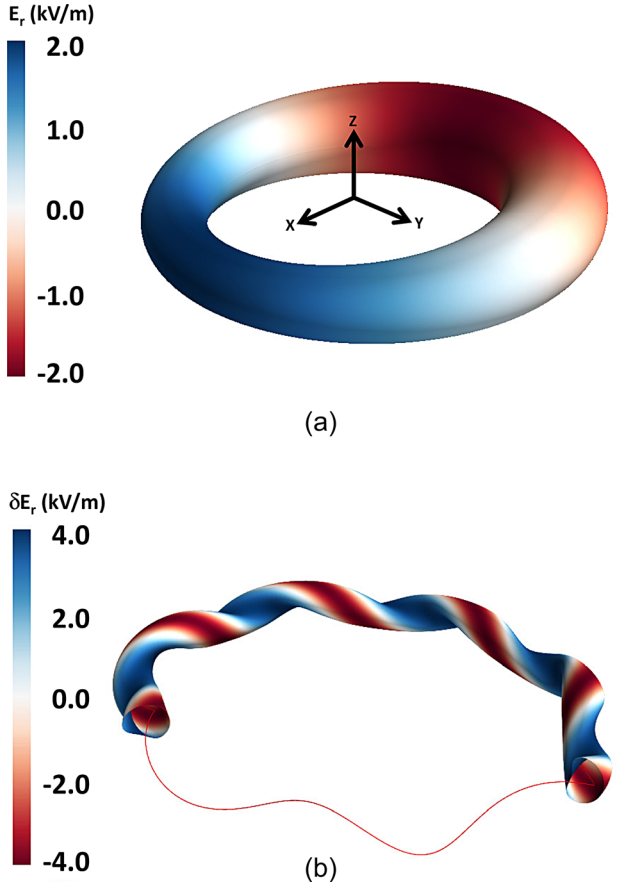

FIG. 3. (a) Measurements of $E^r \approx v_\phi B_\theta$ mapped onto an edge flux surface calculated with VMEC/V3FIT in the 0/1 symmetry; (b) δE^r measured with the array of internal sensors (ISIS), mapped onto a helical flux surface calculated with VMEC/V3FIT.

This article is copyrighted as indicated in the article. Reuse of AIP content is subject to the terms at: http://scitation.aip.org/termsconditions. Downloaded to IP: 150.178.3.9 On: Tue, 06 May 2014 07:32:21

Internal Sensors).[35] By exploiting the technique of a rotating 1/7 island and the mapping on the helical angle and the VMEC flux surface, one can obtain the picture shown in Fig. 3(b): in this case, helical flux surfaces refer to the RFP state with a helical core, known as "Single Helical Axis"–SHAx.[36] In the SHAx state, even if the island is resonating in the core plasma, the helical ripple at the edge is comparable to the 0/1 case, and it is capable of modulating edge kinetic quantities, as it has already been shown in Fig. 1(b). Again, analogously to Fig. 3(a), the E^r field has the same symmetry as the island, and in this case the potential well appears as a blue ribbon winding up the helical surface (actually, in this case colors refer to δE^r, fluctuation along the average value $\langle E^r \rangle < 0$ always negative along u, no reversal. For a detailed discussion of the ISIS measurements in the helical symmetry of RFX, the reader can refer to Ref. 22).

The pictorial view of Fig. 3 makes immediate that the electrostatic potential is parent to the magnetic topology: in particular, Fig. 3(b) shows an impressive similarity with simulations of ambipolar potential in the stellarator[37] (even if in our case we are dealing with actual measurements mapped onto a helical equilibrium). But Fig. 3 shows also deeper result: the values of E^r are not constant on a flux-surface, meaning that if one searches for an analytic form of the potential, this must not be a flux function, $\Phi \neq \Phi(\psi)$.

Summarizing, experiments show that magnetic islands spontaneously resonating in the reversed-field pinch are associated with macroscopic fluctuations of the flow (up to ≈ 20 km/s); the symmetry is the same as the generating island (1/7 low density, and 0/1 at high density in the RFX), and values of E^r are not constant on a flux-surface. In some cases (0/1 at high density) the coherent fluctuations of the flow are also associated to the Greenwald limit through the mechanism of the stagnation point and the MARFE.

III. TEST-PARTICLE SIMULATIONS

To study the development of an ambipolar potential in a 3D configuration, many approaches can be followed. In the stellarator community, neoclassical calculations with δf Monte Carlo codes are customary: some examples include FORTEC-3D[38,39] and EUTERPE-GSRAKE.[37] Alternatively, one can use a linearized drift-kinetic equation, such as in the case of DKES-PENTA.[40] In the case of chaotic structures of the RFP, an optimal tool is the guiding-center code ORBIT,[18] recently validated against a volume-preserving field line tracer code (NEMATO) on the RFP topology.[26] ORBIT exploits a rather unique feature of the RFP: the precise knowledge of the radial structure (eigenfunction) of the saturated, almost stationary spectrum of tearing modes. Eigenfunctions are evaluated for RFX-mod with the code NCT,[41] which solves the Newcomb's equations[42] in toroidal geometry (the constraint are the magnetic fluctuations measured at the conductive shell). In the case of the TEXTOR tokamak, the input is instead the vacuum solutions of the magnetic field induced by the dynamic ergodic divertor, and the constraint are the current values in the coils.[43] Collisions are implemented as pitch-angle scattering between particles (ions, electrons and C^{4+} impurities), following the Boozer-Kuo approach.[44] Coordinates are the Boozer flux coordinates (ψ_p, θ, ζ), where $\zeta = \phi - \nu(\psi_p, \theta)$, with ν a function which can be determined by the straight-field line condition and the "Boozer" Jacobian.[45] Particles are monoenergetic. Finally, the standard ORBIT perfectly absorbing wall has been modified[46] to take into account recycling, which, at least in the RFX, is almost unity (it means that particles released from the wall make up almost the totality of plasma density[47]).

As a first exercise, we can study the parallel connection length to the wall, $L_\parallel$, for the RFX discharge shown in Fig. 2. The connection length is a standard metric used in the context of tokamak stochastic edge, to determine the topology and width of the scrape-off layer: short-connection length regions are called "laminar" zones, since are characterized by large plasma wall interaction and low electron temperatures, while long-connection length regions are called "ergodic," in the sense that are connected to the core, and are characterized by large heat fluxes and high T_e.[9] First define the domain, limited radially by $\psi_{p,2} < \psi_p < \psi_{p,1}$ (see Fig. 4): we deposit particles (electrons) at $\psi_{p,1} = 0.093$ (*deposit surface*) and we recover them at their exit $\psi_{p,2} = 0.079$ (*recovery surface*). In terms of particle dynamics, $\psi_{p,1}$ is $\sim 2\rho_i$ ion gyroradii from the wall $\psi_{p,w}$ (orange, dash-dotted line), while $\psi_{p,2} \sim 9\rho_i$ from the wall. The whole radial domain is $7\rho_i$ wide. The choice of letting particle diffuse backwards is due to the fact that we want particles be recycled on the wall. The domain is divided into a grid $(\zeta_i, \psi_{p,j})$, and $L_\parallel(\zeta_i, \psi_{p,j}) = v_{th}\tau_{trav}$, where τ_{trav} is the travel time for 50% of the initial 1000 electrons to get from the deposit surface on the slice $\zeta = \zeta_i$ to a series of intermediate stops $\psi_{p,j}$, until they get to the final stop (=recovery surface). The poloidal angle θ is random and is not considered in this evaluation. Electron energy is 260 eV and collision frequency (normalized to toroidal transit) is $\nu_e \tau_{tor} = 1.42$. In tokamaks, usually $L_\parallel$ is defined simply as the path integral of the magnetic field line to the wall from $(\psi_{p,1}, \zeta_i)$:[8] here instead we use particles, since our assumption is that the electric field be determined

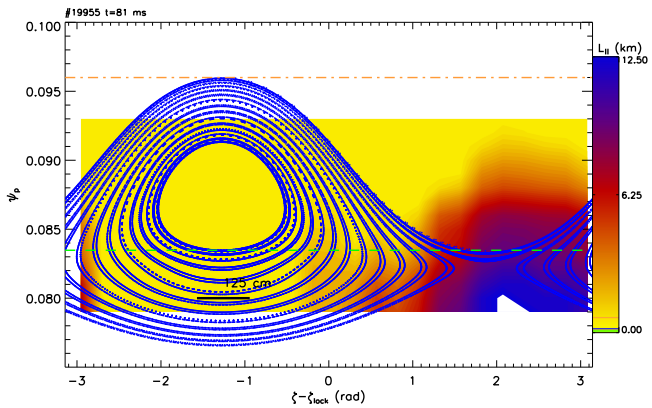

FIG. 4. Contour plot of the connection length $L_\parallel$ defined as the distance (parallel to the magnetic field) travelled by electrons from the deposit surface $\psi_{p,1} = 0.093$ to the recovery surface $\psi_{p,2} = 0.079$. The map describes $L_\parallel(\zeta_i, \psi_{p,j})$, each point $(\zeta_i, \psi_{p,j})$ of the grid being the initial toroidal angle and an intermediate radius, where $L_\parallel$ is recorded. The dashed, horizontal line corresponds to the reversal surface, the dash-dotted line to the wall, $\psi_p = \psi_{p,w}$. Overplotted, a Poincaré section of the 0/1 island. The Poincaré is done with the 0/1 mode only, the $L_\parallel$ with the full spectrum of tearing modes.

This article is copyrighted as indicated in the article. Reuse of AIP content is subject to the terms at: http://scitation.aip.org/termsconditions. Downloaded to IP: 150.178.3.9 On: Tue, 06 May 2014 07:32:21

by a two-fluid effect of electrons and ions (for more details on this calculation, see Ref. 48).

Results for $L_\parallel$ are shown as a color map in Fig. 4. To facilitate the comparison with the magnetic topology, an equatorial Poincaré section is overplotted. The Poincaré is done with the 0/1 mode only, to highlight the dominant helicity, while $L_\parallel$ is calculated with the full mode spectrum. There is a modulation of $L_\parallel$ with the same symmetry of the 0/1 mode. Two regions can be seen: a low-connection length region (10–100 m), corresponding to the O-point (OP) of the island, and a long-connection length region ($L_\parallel > 10$ km) near the X-point (XP). We can think of the RFX edge as composed of a "laminar" and "ergodic" region, similarly to the tokamak. It is worth noting that a similarity with tokamaks, with a separation in laminar and ergodic regions along the helical angle, can be drawn also in the helical, 1/7 state of the RFX, as shown in Ref. 22. The physical reason is that electron orbits have a longer period around the XP: this is the classical pendulum, which shows a period diverging to infinity as approaching the XP along the separatrix, $T_{XP} \to \infty$.[49] With $m = 1$ perturbations to the 0/1 island[1] and electron collisions, the period around the XP does not diverge, but it is still larger than the period around the OP. In addition to this, the 0/1 island touches the wall,[48] so that the period around the OP is further decreased.

To check if the result on electron connection length in the RFX has a general validity, we perform the same type of analysis on the TEXTOR tokamak, simulating a discharge with a resonant magnetic perturbation of helicity 3/1. Results are shown in Fig. 5(a), with the map of electron $L_\parallel$ overplotted to the Poincaré section of the chaotic field produced by the RMP (in this case, the x-axis is the poloidal angle θ). The Poincaré shows a chain of "main islands," with 3/1 periodicity resonating at $\psi_p/\psi_{p,w} \approx 0.82$, and a chain of sidebands ("remnant islands") with periodicity 4/1 resonating at $\psi_p/\psi_{p,w} \approx 0.90$. The presence of two chains of islands in TEXTOR, compared to only one big island in the RFX edge, is due to the different q profile, and to the unavoidable presence of higher sidebands produced by the ergodic divertor of TEXTOR, as compared to the more sophisticated system of feedback control of RFX-mod, where individual modes can be triggered and sidebands are damped while acting on a single mode.[50] Even if the geometry of the fields in RFX and TEXTOR is different, the results are similar: electrons (energy $30 - 100$ eV, depending on radius, and thermal collisions with the background $\nu_e \tau_{tor} = 1.5$) stick in limited portions of the plasma, with a $\sim$3 order of magnitude modulation of $L_\parallel$ that retains the geometry of the parent island [see Fig. 5(a)]. Long radial pathways of short connection length (blue stripes in the online version) are visible between the plasma core and the wall: those are the so-called *laminar flux tubes* that in EMC3-EIRENE simulations (and in measurements) show lower T_e and n_e and fast parallel transport to the wall:[9] an enhanced electron diffusion in the laminar flux-tubes, which is shown by ORBIT, is compatible with the results of EMC3-EIRENE. It is worth noting that, in TEXTOR, the electron period around the OP is larger than that on the XP, which is exactly the opposite than in RFX. This can be due to the different level of magnetic chaos: when increasing perturbations the hyperbolic fixed points become seeds for stochastization.[49] This is anyway an open issue to be clarified, e.g., with a scan as a function of perturbation amplitude.

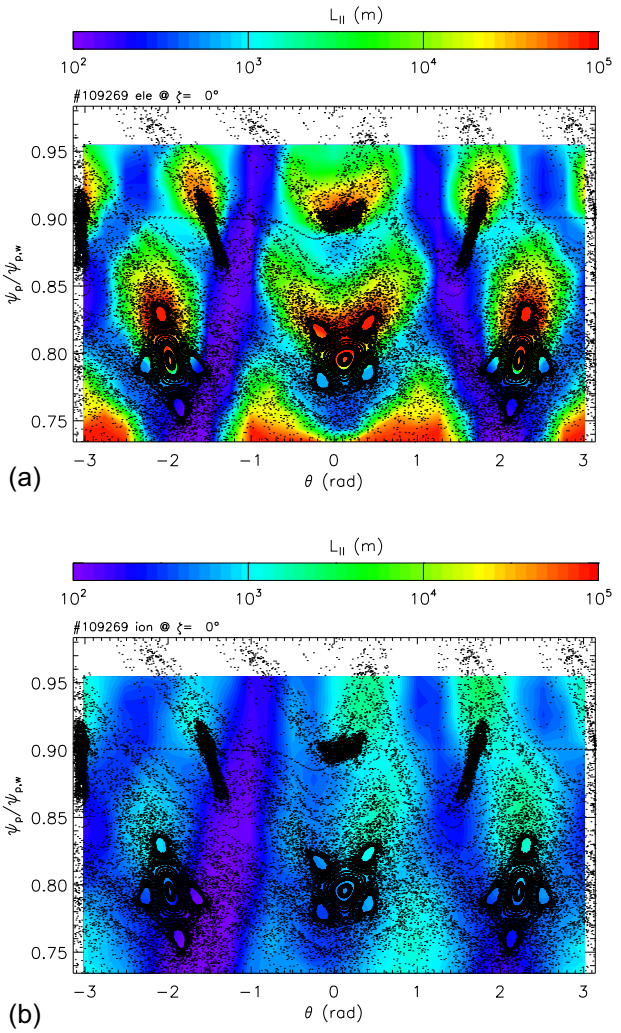

FIG. 5. (a) Electron connection length $L_\parallel$ in the case of TEXTOR (shot # 109269, imposed perturbation of symmetry 3/1); (b) the same, for ions. Note that in the Tokamak the direction perpendicular to the $\vec{B}$ field and radius is the poloidal angle θ, which is on the x-axis in both plots.

In the case of TEXTOR, where the results on the RMPs are consolidated, and electrons follow the standard picture of ergodic fingers, we also performed a calculation of $L_\parallel$ for ions (energy $50 - 100$ eV and thermal collisions $\nu_i \tau_{tor} = 1.5$), which is shown in Fig. 5(b). Overall, the pattern does not change, and ergodic fingers are visible also in the ion map, but there is barely one order of magnitude difference between the OP and the XP of the islands. Ions have larger drifts, larger Larmor radii, and average out the details of the RMPs.

The difference between the ion and electron $L_\parallel$ can be quantified, with a local evaluation of the diffusion coefficients, D_e and D_i, choosing one of the chains of islands (we chose the 4/1, i.e., the "remnant" islands). This evaluation includes the effects of magnetic topology, drifts and collisions: it catches the whole neoclassical behavior, plus the effect of the ergodic magnetic field. Start evaluating steady state distributions $n(\psi)$ by fixing source and sink:[51] choose a small helical domain, reinsert lost particles at the center with uniform pitch. Since the domain is helical, the "center" means a helical surface at a

This article is copyrighted as indicated in the article. Reuse of AIP content is subject to the terms at: http://scitation.aip.org/termsconditions. Downloaded to IP: 150.178.3.9 On: Tue, 06 May 2014 07:32:21

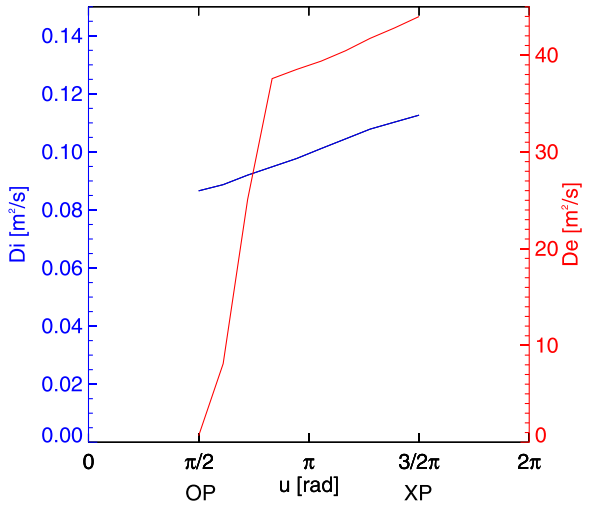

FIG. 6. Local electron and ion diffusion coefficient, as a function of the helical angle $u = m\theta - n\zeta + \phi_{m,n}$, in the case of TEXTOR. The OP corresponds to $u = \pi/2$, the XP to $u = 3/2\pi$.

given helical angle u (for example, $u = \pi/2$ means the OP, $u = 3/2\pi$ means the XP). Finally, D is given by the ratio between the flux and the density gradient. By repeating the evaluation over an array of u values, one can obtain the plot shown in Fig. 6. For ions, D_i is almost neoclassical, $D_i \approx 0.1\,\mathrm{m}^2/\mathrm{s}$, slightly increasing when moving along the helical angle from the OP to the XP. For electrons, D_e is of the order $10\,\mathrm{m}^2/\mathrm{s}$, which is a typical value in a stochastic magnetic field.[51] Therefore, $D_e \gg D_i$ everywhere, but D_e depends also strongly on u: there is one order of magnitude difference between the OP and the XP, from 4 to 40 m^2/s. This, on the one hand quantifies the effect of the ergodic fingers; on the other hand, it shows a strong dependence of D_e on the parent magnetic resonance associated with chaos.

The standard picture with RMPs is that $D_e \gg D_i$, and thus electrons are rapidly lost, determining the so-called "density pump-out.".[52] On the basis of what shown with ORBIT, the picture of the density pumpout is really over-simplified: a strong potential builds up to balance radial diffusion and get ambipolarity $\Gamma_e = \Gamma_i$. In fact, a modification of E^r is generally observed in tokamaks during RMP application.[53,54] Moreover, due to the strong helical modulation of D_e, the potential is expected to have the same symmetry as the original m/n mode. Since it depends on the drifts, which are proportional to $\rho = mv/eB$, the potential is expected to be also energy-dependent.

IV. THE AMBIPOLAR MODEL

On the basis of the results of the preceding sections, we can build up a model of electrostatic potential to include in ORBIT to get the ambipolar condition $\Gamma_e = \Gamma_i$ at the recovery surface $\psi_{p,2}$. The simplest geometry is that of RFX with the 0/1 mode, so that the helical angle is simply $u = -\zeta$ [Figs. 2–4]. The approach exploits the fact that the GC Hamiltonian can be written as $H = 1/2\rho_\parallel^2 B^2 + \mu B + \Phi$, where $\rho_\parallel = v_\parallel/B$ and μ is the magnetic moment: in this way, if an analytical guess of the potential is available, Φ can be added easily to the GC equations of motion.[18] This is not a self-consistent approach, but it is easy to implement, and requires small computational time, since electron and ion simulations can be run separately. Since Φ is a model of ambipolar potential, it will be described on the plane perpendicular to the equilibrium field, which in the RFP edge is B^θ. Therefore, $\Phi = \Phi(\psi_p, \zeta)$ and $\partial\Phi/\partial\theta = 0$.

The radial profile of the model Φ can be derived from existing data from Langmuir probes, showing that E^r has an almost constant value in the region $0.85 < r/a < 1$, and changes sign according to the phase of the 0/1 mode [see Fig. 7(a), which is adapted from Ref. 29]. Therefore, as model for E^{ψ_p} we take

$$E^{\psi_p} = E_a + \frac{1}{2}E_{r,w}\left[\tanh\left(\frac{\psi_p - \psi_{p,rv}}{\sigma_{\psi_p}}\right) + 1\right], \qquad (1)$$

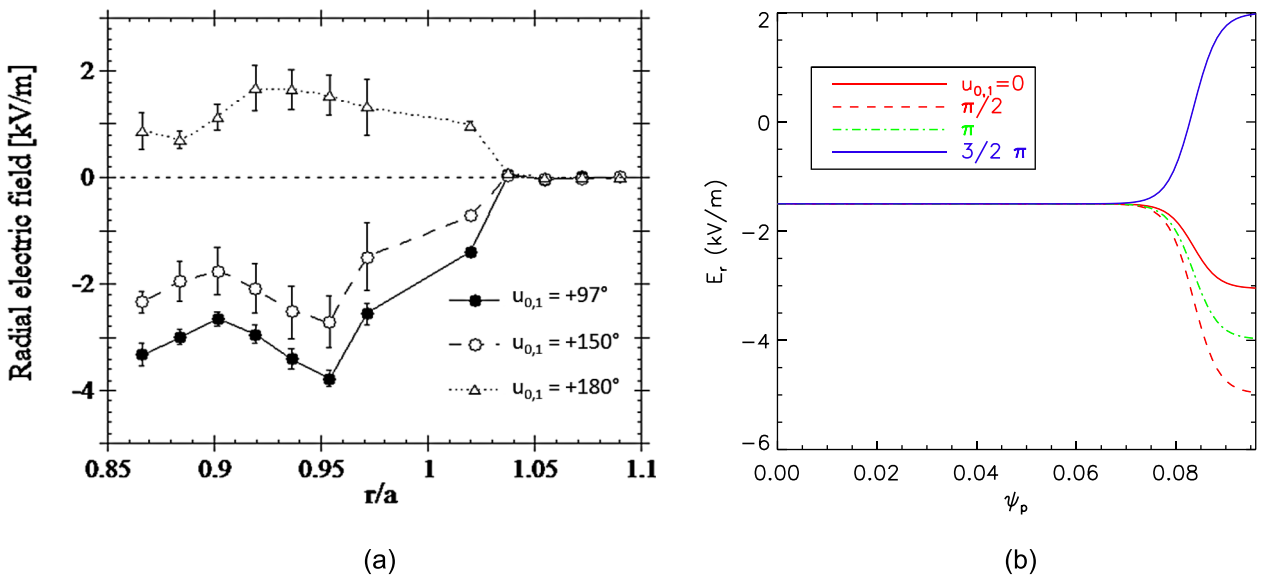

FIG. 7. (a) Experimental radial profiles of the radial electric field E^r, at different helical phases $u_{0,1}$; (b) The model for E^r derived from measurements.

This article is copyrighted as indicated in the article. Reuse of AIP content is subject to the terms at: http://scitation.aip.org/termsconditions. Downloaded to IP: 150.178.3.9 On: Tue, 06 May 2014 07:32:21

where $\psi_{p,rv}$ is the reversal surface (resonance of the 0/1 mode and therefore center of the potential well), and $\sigma_{\psi p}$ is the radial (half) width of the potential well, chosen to be $\sim 2.5\rho_i$. This choice is consistent with Fig. 7(a) and the width of the domain in Fig. 4 (in fact, $\psi_{p,1} - \psi_{p,2} \sim 2\sigma_{\psi_p}$). Equation (1) takes the form of Fig. 7(b), dashed-triple dotted line: in the potential well (=center of the convective cell) the radial electric field in the edge is *positive*, and changes sign at $\psi_p = \psi_{p,rv} - \sigma_{\psi_p} = 0.077$, which corresponds to ~ 38 cm ($r/a = 0.83$). In Eq. (1), the value E_a is chosen to match the values of $E_r(a)$ far from the convective cell [open circles in Fig. 7(a)], and is a value that levels off in the core (it does not make any role in computations, since our simulations never explore $\psi_p < 0.079$). In the end, the only free parameter left is $E_{r,w}$, which plays the role of the *amplitude* of the ambipolar potential.

The angular dependence is derived from the GPI data shown in Fig. 2, and is modeled as

$$\mathcal{A}(\zeta) = 2e^{-(\zeta-\zeta_0)^2/2\sigma_\zeta^2} - 1\,, \tag{2}$$

which fundamentally is a 0/1 dependence along the toroidal angle ζ (the same as the helical angle), with the possibility of choosing the toroidal amplitude of the potential well, σ_ζ. Following the GPI data, we choose $\sigma_\zeta = 50^\circ$ (whole width 100° toroidally). The free parameter in Eq. (2) is the *phase* of the ambipolar potential, ζ_0.

By combining Eqs. (1) and (2), one obtains

$$\Phi(\psi_p, \zeta) = -E_a\psi_p + V(\psi_p) \times \mathcal{A}(\zeta)\,, \tag{3}$$

where $V(\psi_p)$ is the integral of (1),

$$V(\psi_p) = -\frac{1}{2}E_{r,w}\left[\sigma_{\psi_p}\log\left(\cosh\left(\frac{\psi_p - \psi_{p,rv}}{\sigma_{\psi_p}}\right)\right) + \psi_p\right]. \tag{4}$$

Details of the derivation of this model can be found in Ref. 46. A contour plot of the potential in Eq. (3) is shown in Fig. 8(a), for a guess of the phase $\zeta_0 = 3/2\pi$. In the edge, a potential hill (at $\zeta = \zeta_0 - \pi$) and a potential well (at $\zeta = \zeta_0$) are visible. Looking more in detail (white inset), a feature of our potential model is the presence of a saddle point at $\zeta = \zeta_0$: along the radius the potential shows a peak at $\psi_p = \psi_{p,rv}$, while along the angle it has a minimum at $\zeta = \zeta_0$, which is evident as an X-shaped contour in the inset of Fig. 8(a). Actually, the equipotential surfaces already define the shape of the convective cell measured by the GPI in RFX, and the $\vec{E} \times \vec{B}$ flow can be defined as the motion of electrons and ions along the equipotential surfaces, $\vec{v}_{E\times B} \cdot \nabla\Phi = 0$, that conserves kinetic energy and can drive the macroscopic transport features which are seen near the Greenwald limit.[15–17] The presence of the convective cell is made evident by differentiating Eq. (3), and obtaining the map of (E^ζ, E^{ψ_p}), shown in Fig. 8(b) as the expanded inset of panel (a): the radial electric field is negative, except for the inner part of the convective cell, where $E^r > 0$.

The analytical model for the potential can now be used to get ambipolarity in ORBIT runs: the domain is the same as in Fig. 4, with $\psi_{p,2} < \psi_p < \psi_{p,1}$. The technique is similar to that used in the stellarator community: vary the free parameters until $\Gamma_e = \Gamma_i$ (the "root" in the stellarator jargon). Our case is only slightly more complicated, since we have two parameters, amplitude and phase. To determine the potential amplitude, we start from a basic requirement of the potential: it must be able to trap electrons. We vary the free parameter $E_{r,w}$ in single-particle runs (no perturbations), until electrons are trapped around $\zeta = \zeta_0 - \pi$ (the potential hill). We vary then the electron energy, and obtain another value of the amplitude. We can then compute the radial electric field at the wall, $E^{\psi_p}(\psi_w) = E_a - E_{r,w}$, as a function of the electron energy: the result is shown in Fig. 9(a), which is the rather expected linear dependence with energy. In fact, we can expect the radial electric field to be $E^{\psi_p}(\psi_w) = -T_e/2e\sigma_{\psi_p}$.

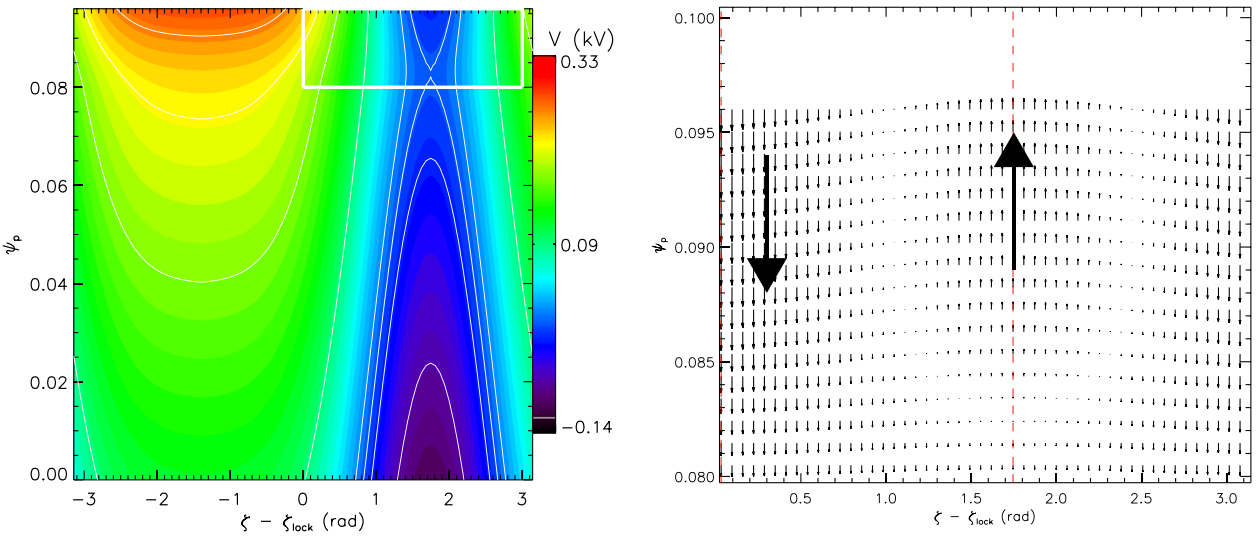

FIG. 8. (a) Contour plot of the model of potential, in the 0/1 symmetry. The phase has been chosen as $\zeta_0 = 3/2\pi$, in order to match the experimental data. The white inset encloses the region of the convective cell measured by the GPI diagnostic, shown in Fig. 2; (b) By differentiating the potential, we get the electric field in the plane perpendicular to $\vec{B}$, with its two components (E^ζ, E^r). Note that the region of $E^r > 0$ corresponds to the center of the cell, or, equivalently, to the potential well.

This article is copyrighted as indicated in the article. Reuse of AIP content is subject to the terms at: http://scitation.aip.org/termsconditions. Downloaded to IP: 150.178.3.9 On: Tue, 06 May 2014 07:32:21

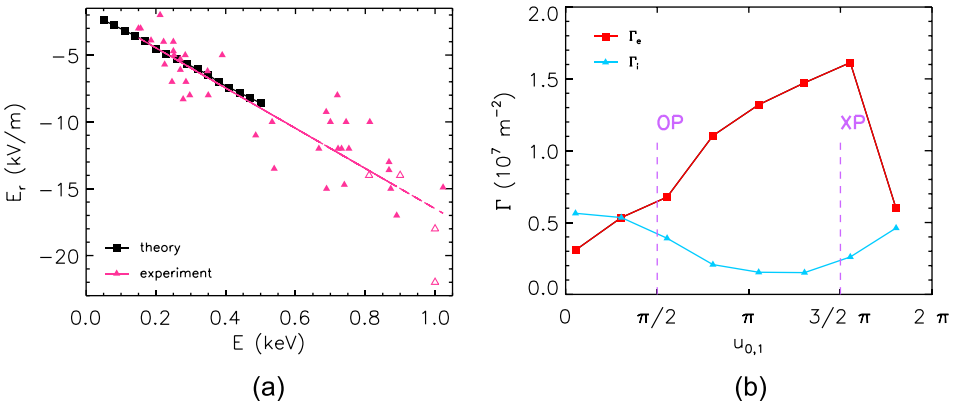

FIG. 9. Determination of the potential amplitude and phase: (a) Radial electric field at the wall as a function of electron energy (code: squares, data: triangles); (b) electron and ion fluxes as a function of the potential phase. The phase has been expressed in terms of helical angles, so that $u_{0,1} = \pi/2$ corresponds to the OP of the 0/1 island, while $u_{0,1} = 3/2\pi$ corresponds to the XP (the same as in Figs. 2 and 4). ORBIT gives as a result of an ambipolar condition an amplitude well in agreement with data, but a phase which corresponds to the OP of the island, and not the XP, as in Fig. 2.

Inserting the numerical value for σ_{ψ_p}, one obtains the values shown in Fig. 9(a). We can also evaluate E^r from the GPI measurements of flow, and neglecting the diamagnetic term. The result is the triangles (purple in the online version) of Fig. 9(a). There is a striking agreement between theory and experiment, showing that the E^r field at the edge of RFX is likely to be ambipolar.

The phase can now be determined with the standard technique: for $E = 260\,\text{eV}$ we get $E_{r,w} = 4\,\text{kV/m}$, and ζ_0 is a free parameter. Let 6×10^4 particles diffuse between the deposit $\psi_{p,1}$ and the recovery surface $\psi_{p,2}$, subject to the full spectrum of perturbations and collisions (pitch angle scattering only). Each run is performed by varying ζ_0: look at the fluxes Γ_e and Γ_i at the recovery surface, and find a "root" $\Gamma_e = \Gamma_i$ as a function of ζ_0. The result is shown in Fig. 9(b) as a function of the helical phase $u_{0,1}$ (given by $u_{0,1} = -\zeta_0$). There is one root, and ambipolarity is reached at $u \approx \pi/2$, i.e., when the potential well is in the proximity of the OP of the magnetic island. The result is not unreasonable, since the potential well means $E^r > 0$ [see Fig. 8], and a positive electric field avoids further losses of electrons where D_e is already large, as seen in Tokamaks with the RMP.[10] Indeed, measurements of the plasma potential in TEXTOR with the application of the 3/1 RMP, show that the potential well corresponds to the region with larger D_e, i.e., the ergodic fingers.[55] Nevertheless, measurements in RFX show the opposite, the potential well stays at the XP of the 0/1 island [Fig. 2].

There can be many reasons for this mismatch, and we will discuss them briefly in the Conclusions. The main issue is with energy-exchanging collisions: as shown above, the potential amplitude is critically dependent on electron energy. Whatever mechanism increases electron energy or determines a scattering of energies, can influence the potential. While developing an energy scattering operator in ORBIT, in April 2013, we performed an experimental scan on collisions. In RFX, the 1/7, helical state is obtained at high current and low density, and it is extremely difficult to obtain it at high density (it disappears at rather modest Greenwald fractions, $n/n_G \gtrsim 0.35$ (Ref. 48)). On the contrary, a large amplitude 0/1 mode is spontaneously obtained at high density ($n/n_G = 0.8$). Therefore, we performed a campaign where we reproduced a robust 0/1 mode at low density ($n/n_G = 0.2$), through a combined feedback action on both $m = 1$ and $m = 0$ modes, and carefully tailoring the size of the island to be similar to the high density case [shown, e.g., in Fig. 2]. This careful tuning of the island size implies also a feedback control of the edge q, which is a recent accomplishment in the RFX-mod experiment.[56] Results are shown in Fig. 10: on the top row, the Poincaré plots of the two islands in the (u, ψ_p) plane, 0/1 on the left, and 1/7 on the right, are shown. The maps show that, in the helical angle, islands that in principle should look quite different, possess in reality an analogous topology, which reflects the similarity of their respective field-line Hamiltonians, when expressed in action-angle variables.[26] In particular, the size of the edge ripple is similar. On the bottom row, the flow as a function of the helical angle u is shown: on the left, in the 0/1 case, the GPI measurements at high and low collisions (blue and red, respectively, in the online version of the paper); on the right, the 1/7 case, low collisions, with combined flow measurements with the GPI and ISIS diagnostics. The result is striking: whatever symmetry of islands and collisional regime, the potential well of RFX sits near the XP of the islands. This remains an open issue.

V. CONCLUSIONS AND PERSPECTIVES

Measurements of flow in the edge of the RFX-mod reversed field pinch show macroscopic modulations in presence of magnetic islands with a definite symmetry. The use of the helical angle $u = m\theta - n\phi + \omega t$ allows for clarifying in detail the relationship between magnetic island and flow,[22] in two different geometries, and to map them on the helical flux surfaces with unprecedented detail for a measurement of this type. In this paper we have proposed a model of ambipolar potential with the code ORBIT which explains the electrostatic response to magnetic islands: the rationale of the model is the marked dependence of electron diffusion on the symmetry of the magnetic islands. The model of the potential correctly explains the geometry and amplitude of the potential in RFX, while the phase is π-shifted with respect to measurements. Recent experiments confirm this mismatch. It is worth noting anyway that measurements of the plasma potential in TEXTOR with the application of a resonant 3/1 perturbation, show that the potential well corresponds to the region with larger D_e, which would be consistent with the results of ORBIT.[55] This issue with the phases could be ascribed to a collisional dependence (the 0/1

This article is copyrighted as indicated in the article. Reuse of AIP content is subject to the terms at: http://scitation.aip.org/termsconditions. Downloaded to IP: 150.178.3.9 On: Tue, 06 May 2014 07:32:21

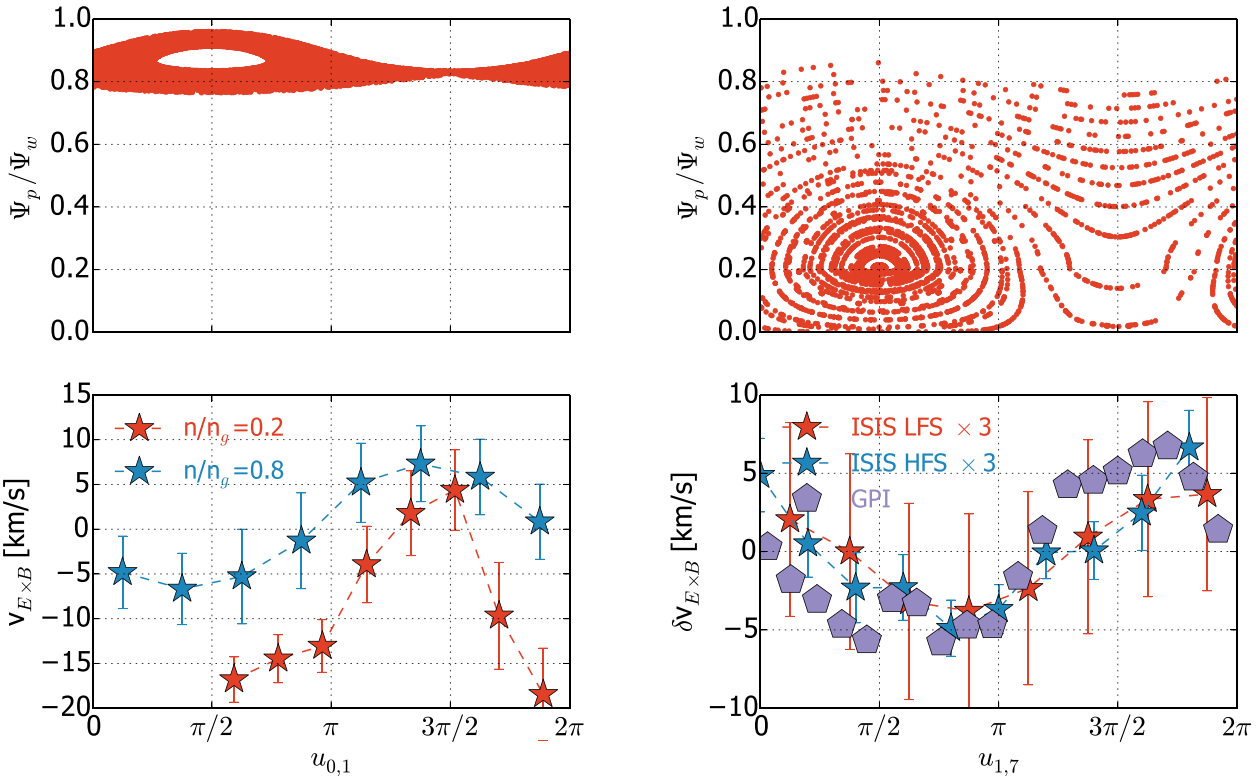

FIG. 10. Summary of experimental results in the RFX-mod: (top) Poincaré plots of islands, as a function of the helical angle and ψ_p (0/1 on the right, 1/7 on the left); (bottom) measurements of flow as a function of the helical angle, 0/1 on the right, 1/7 on the left. In the 0/1 case, two different values of density are reported, $n/n_G = 0.8$ (blue stars) and $n/n_G = 0.2$ (red stars). The phase of the flow, with respect to the island, seems to be independent of collisionality in experiment.

case of RFX is highly collisional, contrary to TEXTOR); to a different level of chaos, in RFX compared to TEXTOR; or to a more pronounced plasma-wall interaction (measured particle fluxes to the wall in the reversed-field pinch (RFP) are 2 orders of magnitude larger than in tokamaks, being $\sim 10^{20} m^{-2} s^{-1}$ (Ref. 47)).

Future plans include the introduction in ORBIT of energy-exchanging collisions with a full profile background, following the Boozer-Kuo scheme.[44] In fact, as explained in this paper, the whole mechanism of the electrostatic potential is based on particle trapping and detrapping in a potential well: energy-exchanging collisions are therefore a fundamental ingredient in determining the correct form of the potential. In fact, recent simulations with FORTEC-3D on the LHD stellarator show marked differences when considering a Maxwellian against a monoenergetic population: in particular, the typical divergence of the neoclassical ion flux for $E^r = 0$ disappears in Maxwellian runs.[39] The use of a Maxwellian and full-profile collisions should allow to cast some light on the phase conundrum, RFX vs TEXTOR, but also to explore the collisional dependence of RMP application.[19] Finally, it should allow to simulate energetic electron tails, such those produced by electron cyclotron heating (ECRH): in fact, since the 1980s the electrostatic E^r was seen to depend on ECRH.[57]

ACKNOWLEDGMENTS

This work was supported by the European Communities under the contract of Association between EURATOM/ENEA (contract FU07-CT-2007-00053) and EURATOM/FZJ. This work was partially supported by the U.S. Department of Energy Grant DE-AC02-09CH11466.

[1]G. Spizzo, S. Cappello, A. Cravotta, D. F. Escande, I. Predebon, L. Marrelli, P. Martin, and R. B. White, Phys. Rev. Lett. **96**, 025001 (2006), http://link.aps.org/abstract/PRL/v96/e025001.
[2]K. Ida, N. Ohyabu, T. Morisaki, Y. Nagayama, S. Inagaki, K. Itoh, Y. Liang, K. Narihara, A. Y. Kostrioukov, B. J. Peterson *et al.* (LHD Experimental Group), Phys. Rev. Lett. **88**, 015002 (2001), http://link.aps.org/doi/10.1103/PhysRevLett.88.015002.
[3]T. E. Evans, R. A. Moyer, K. H. Burrell, M. E. Fenstermacher, I. Joseph, A. W. Leonard, T. H. Osborne, G. D. Porter, M. J. Schaffer, P. B. Snyder *et al.*, Nature Phys. **2**, 419 (2006), http://dx.doi.org/10.1038/nphys312.
[4]W. Suttrop, T. Eich, J. C. Fuchs, S. Günter, A. Janzer, A. Herrmann, A. Kallenbach, P. T. Lang, T. Lunt, M. Maraschek *et al.* (ASDEX Upgrade Team), Phys. Rev. Lett. **106**, 225004 (2011), http://link.aps.org/doi/10.1103/PhysRevLett.106.225004.
[5]K. Finken, S. Abdullaev, A. Kaleck, and G. Wolf, Nucl. Fusion **39**, 637 (1999), http://stacks.iop.org/0029-5515/39/i=5/a=306.
[6]A. Loarte, B. Lipschultz, A. Kukushkin, G. Matthews, P. Stangeby, N. Asakura, G. Counsell, G. Federici, A. Kallenbach, K. Krieger *et al.*, Nucl. Fusion **47**, S203 (2007), http://stacks.iop.org/0029-5515/47/i=6/a=S04.
[7]S. S. Abdullaev, A. Wingen, and K. H. Spatschek, Phys. Plasmas **13**, 042509 (2006), http://link.aip.org/link/?PHP/13/042509/1.
[8]O. Schmitz, M. Jakubowski, H. Frerichs, D. Harting, M. Lehnen, B. Unterberg, S. Abduallaev, S. Brezinsek, I. Classen, T. Evans *et al.*, Nucl. Fusion **48**, 024009 (2008), http://stacks.iop.org/0029-5515/48/i=2/a=024009.
[9]H. Stoschus, O. Schmitz, H. Frerichs, D. Reiser, M. Jakubowski, B. Unterberg, M. Lehnen, D. Reiter, U. Samm, and the TEXTOR team, Nucl. Fusion **52**, 083002 (2012), http://stacks.iop.org/0029-5515/52/i=8/a=083002.
[10]V. Rozhansky, E. Kaveeva, P. Molchanov, I. Veselova, S. Voskoboynikov, D. Coster, A. Kirk, S. Lisgo, and E. Nardon, Nucl. Fusion **50**, 034005 (2010), http://stacks.iop.org/0029-5515/50/i=3/a=034005.

This article is copyrighted as indicated in the article. Reuse of AIP content is subject to the terms at: http://scitation.aip.org/termsconditions. Downloaded to IP: 150.178.3.9 On: Tue, 06 May 2014 07:32:21

[11]Y. Xu, R. R. Weynants, S. Jachmich, M. Van Schoor, M. Vergote, P. Peleman, M. W. Jakubowski, M. Mitri, D. Reiser, B. Unterberg *et al*. (the TEXTOR Team), Phys. Rev. Lett. **97**, 165003 (2006), http://link.aps.org/doi/10.1103/PhysRevLett.97.165003.
[12]W. R. Hess, C. DeMichelis, M. Mattioli, F. Clairet, M. Druetta, A. Grosman, R. Guirlet, T. Hutter, J. Lasalle, and P. Monier-Garbet, Plasma Phys. Controlled Fusion **37**, 951 (1995), http://stacks.iop.org/0741-3335/37/i=9/a=003.
[13]H. Maaßberg, C. D. Beidler, and E. E. Simmet, Plasma Phys. Controlled Fusion **41**, 1135 (1999), http://stacks.iop.org/0741-3335/41/i=9/a=306.
[14]S. Ortolani and RFX Team, Plasma Phys. Controlled Fusion **48**, B371 (2006), http://stacks.iop.org/0741-3335/48/i=12B/a=S34.
[15]M. E. Puiatti, P. Scarin, G. Spizzo, M. Valisa, R. Paccagnella, I. Predebon, M. Agostini, A. Alfier, A. Canton, S. Cappello *et al*., Phys. Plasmas **16**, 012505 (2009), URL http://link.aip.org/link/?PHP/16/012505/1.
[16]M. E. Puiatti, P. Scarin, G. Spizzo, M. Valisa, M. Agostini, A. Alfier, A. Canton, L. Carraro, E. Gazza, R. Lorenzini *et al*., Nucl. Fusion **49**, 045012 (2009), URL http://stacks.iop.org/0029-5515/49/045012.
[17]G. Spizzo, P. Scarin, M. Agostini, A. Alfier, F. Auriemma, D. Bonfiglio, S. Cappello, A. Fassina, P. Franz, L. Piron *et al*., Plasma Phys. Controlled Fusion **52**, 095011 (2010), http://stacks.iop.org/0741-3335/52/i=9/a=095011.
[18]R. B. White and M. S. Chance, Phys. Fluids **27**, 2455 (1984), http://link.aip.org/link/?PFL/27/2455/1.
[19]P. Lang, A. Loarte, G. Saibene, L. Baylor, M. Becoulet, M. Cavinato, S. Clement-Lorenzo, E. Daly, T. Evans, M. Fenstermacher *et al*., Nucl. Fusion **53**, 043004 (2013), http://stacks.iop.org/0029-5515/53/i=4/a=043004.
[20]R. Moyer, M. V. Zeeland, D. Orlov, A. Wingen, T. Evans, N. Ferraro, J. Hanson, R. Nazikian, M. Wade, and L. Zeng, Nucl. Fusion **52**, 123019 (2012), http://stacks.iop.org/0029-5515/52/i=12/a=123019.
[21]R. Paccagnella, S. Ortolani, P. Zanca, A. Alfier, T. Bolzonella, L. Marrelli, M. E. Puiatti, G. Serianni, D. Terranova, M. Valisa *et al*., Phys. Rev. Lett. **97**, 075001 (2006), http://link.aps.org/abstract/PRL/v97/e075001.
[22]N. Vianello, G. Spizzo, M. Agostini, P. Scarin, L. Carraro, R. Cavazzana, G. De Masi, E. Martines, B. Momo, C. Rea *et al*., Nucl. Fusion **53**, 073025 (2013), http://stacks.iop.org/0029-5515/53/i=7/a=073025.
[23]Y. Feng, M. Kobayashi, T. Lunt, and D. Reiter, Plasma Phys. Controlled Fusion **53**, 024009 (2011), http://stacks.iop.org/0741-3335/53/i=2/a=024009.
[24]M. Agostini, R. Cavazzana, P. Scarin, and G. Serianni, Rev. Sci. Instrum. **77**, 10E513 (2006); papers from the 16th Topical Conference on High Temperature Plasma Diagnostics, Williamsburg, Virginia, USA, May 2006, http://link.aip.org/link/?RSI/77/10E513/1.
[25]M. Agostini, P. Scarin, R. Cavazzana, F. Sattin, G. Serianni, M. Spolaore, and N. Vianello, Plasma Phys. Controlled Fusion **51**, 105003 (2009), http://stacks.iop.org/0741-3335/51/i=10/a=105003.
[26]G. Ciaccio, M. Veranda, D. Bonfiglio, S. Cappello, G. Spizzo, L. Chacon, and R. B. White, Phys. Plasmas **20**, 062505 (2013), http://link.aip.org/link/?PHP/20/062505/1.
[27]R. Bartiromo, Phys. Plasmas **5**, 3342 (1998), http://link.aip.org/link/?PHP/5/3342/1.
[28]G. De Masi, E. Martines, M. Spolaore, N. Vianello, R. Cavazzana, P. Innocente, B. Momo, S. Spagnolo, and M. Zuin, Nucl. Fusion **53**, 083026 (2013), http://stacks.iop.org/0029-5515/53/i=8/a=083026.
[29]M. Puiatti, L. Tramontin, V. Antoni, R. Bartiromo, L. Carraro, D. Desideri, E. Martines, F. Sattin, P. Scarin, G. Serianni *et al*., J. Nucl. Mater. **290–293**, 696 (2001); Proceedings of 14th International Conference on Plasma-Surface Interactions in Controlled Fusion Devices (PSI-14), Rosenheim, Germany, May 2000, http://www.sciencedirect.com/science/article/B6TXN-42K5JDD-5R/2/feb4d0596875168b657df4fac2847169.
[30]L. Carraro, M. Puiatti, F. Sattin, P. Scarin, M. Spolaore, M. Valisa, B. Zaniol, and P. Zanca, J. Nucl. Mater. **313–316**, 976 (2003); Proceedings of 15th International Conference on Plasma-Surface Interactions in Controlled Fusion Devices (PSI-15), Gifu, Japan, May 2002, http://www.sciencedirect.com/science/article/B6TXN-482YXVY-F/2/23116da186189559f6f290380a4fd636.
[31]U. Samm, M. Brix, F. Durodié, M. Lehnen, A. Pospieszczyk, J. Rapp, G. Sergienko, B. Schweer, M. Tokar, and B. Unterberg, J. Nucl. Mater. **266–269**, 666 (1999); Proceedings of 13th International Conference on Plasma-Surface Interactions in Controlled Fusion Devices (PSI-13), San Diego, USA, 1998, http://www.sciencedirect.com/science/article/pii/S0022311598005169.
[32]G. Sergienko, A. Pospieszczyk, M. Lehnen, M. Brix, J. Rapp, B. Schweer, and P. Greenland, J. Nucl. Mater. **290–293**, 720 (2001); Proceedings of 14th International Conference on Plasma-Surface Interactions in Controlled Fusion Devices (PSI-14), Rosenheim, Germany, May 2000, http://www.sciencedirect.com/science/article/pii/S0022311500006036.
[33]M. E. Puiatti, G. Spizzo, M. Agostini, F. Auriemma, D. Bonfiglio, A. Canton, S. Cappello, L. Carraro, R. Cavazzana, G. Ciaccio *et al*., Plasma Phys. Controlled Fusion **55**, 124013 (2013), http://stacks.iop.org/0741-3335/55/i=12/a=124013.
[34]D. Terranova, L. Marrelli, J. Hanson, S. Hirshman, M. Cianciosa, and P. Franz, Nucl. Fusion **53**, 113014 (2013), http://stacks.iop.org/0029-5515/53/i=11/a=113014.
[35]G. Serianni, W. Baker, and S. Dal Bello, Rev. Sci. Instrum. **74**, 1558 (2003); papers from the 14th Topical Conference on High Temperature Plasma Diagnostics, http://link.aip.org/link/?RSI/74/1558/1.
[36]R. Lorenzini, E. Martines, P. Piovesan, D. Terranova, P. Zanca, M. Zuin, A. Alfier, D. Bonfiglio, F. Bonomo, A. Canton *et al*., Nature Phys. **5**, 570 (2009), http://www.nature.com/doifinder/10.1038/nphys1308.
[37]J. M. García-Regaña, R. Kleiber, C. D. Beidler, Y. Turkin, H. Maaßberg, and P. Helander, Plasma Phys. Controlled Fusion **55**, 074008 (2013), http://stacks.iop.org/0741-3335/55/i=7/a=074008.
[38]S. Satake, Y. Idomura, H. Sugama, and T.-H. Watanabe, Comput. Phys. Commun. **181**, 1069 (2010), http://www.sciencedirect.com/science/article/pii/S0010465510000536.
[39]S. Matsuoka, S. Satake, M. Yokoyama, A. Wakasa, and S. Murakami, Phys. Plasmas **18**, 032511 (2011), http://link.aip.org/link/?PHP/18/032511/1.
[40]J. Lore, W. Guttenfelder, A. Briesemeister, D. T. Anderson, F. S. B. Anderson, C. B. Deng, K. M. Likin, D. A. Spong, J. N. Talmadge, and K. Zhai, Phys. Plasmas (1994-present) **17**, 056101 (2010), http://scitation.aip.org/content/aip/journal/pop/17/5/10.1063/1.3300465.
[41]P. Zanca and D. Terranova, Plasma Phys. Controlled Fusion **46**, 1115 (2004), http://stacks.iop.org/0741-3335/46/i=7/a=011.
[42]W. A. Newcomb, Ann. Phys. **10**, 232 (1960), http://www.sciencedirect.com/science/article/B6WB1-4DDR40K-T1/2/72496b9dddbc90fe5a2f659bfbef1ea6.
[43]K. H. Finken *et al*., *The Structure of Magnetic Field in the TEXTOR-DED* (Jülich: Forschungszentrum, Zentralbibliothek, 2005), Vol. 45 of Schriften des Forschungszentrums Jülich. Reihe Energietechnik/energy technology, http://hdl.handle.net/2128/532.
[44]A. H. Boozer, Phys. Fluids **24**, 1999 (1981), http://link.aip.org/link/?PFL/24/1999/1.
[45]R. B. White, *The Theory of Toroidally Confined Plasmas*, 2nd ed. (Imperial College Press, 57 Shelton Street, Covent Garden, London WC2H 9HE, 2006), p. 42, http://www.icpress.co.uk/physics/p440.html.
[46]G. Spizzo, M. Agostini, P. Scarin, N. Vianello, R. B. White, S. Cappello, M. E. Puiatti, M. Valisa, and RFX-mod Team, Nucl. Fusion **52**, 054015 (2012), http://stacks.iop.org/0029-5515/52/i=5/a=054015.
[47]M. Puiatti, G. Spizzo, F. Auriemma, L. Carraro, R. Cavazzana, G. De Masi, M. Gobbin, P. Innocente, I. Predebon, P. Scarin *et al*., Nucl. Fusion **53**, 073001 (2013), http://stacks.iop.org/0029-5515/53/i=7/a=073001.
[48]P. Scarin, N. Vianello, M. Agostini, G. Spizzo, M. Spolaore, M. Zuin, S. Cappello, L. Carraro, R. Cavazzana, G. De Masi *et al*., Nucl. Fusion **51**, 073002 (2011), http://stacks.iop.org/0029-5515/51/i=7/a=073002.
[49]B. V. Chirikov, Phys. Rep. **52**, 263 (1979), http://www.sciencedirect.com/science/article/B6TVP-46SPHBD-5V/2/cf84bfb81360e901a1e2b66baa0d7ce6.
[50]L. Marrelli, P. Zanca, M. Valisa, G. Marchiori, A. Alfier, F. Bonomo, M. Gobbin, P. Piovesan, D. Terranova, M. Agostini *et al*., Plasma Phys. Controlled Fusion **49**, B359 (2007), http://stacks.iop.org/0741-3335/49/B359.
[51]G. Spizzo, R. B. White, S. Cappello, and L. Marrelli, Plasma Phys. Controlled Fusion **51**, 124026 (2009), http://stacks.iop.org/0741-3335/51/i=12/a=124026.
[52]T. Evans, M. Fenstermacher, R. Moyer, T. Osborne, J. Watkins, P. Gohil, I. Joseph, M. Schaffer, L. Baylor, M. Bécoulet *et al*., Nucl. Fusion **48**, 024002 (2008), http://stacks.iop.org/0029-5515/48/i=2/a=024002.
[53]J. Coenen, O. Schmitz, B. Unterberg, M. Clever, M. Jakubowski, U. Samm, B. Schweer, H. Stoschus, M. Tokar, and TEXTOR Team, Nucl. Fusion **51**, 063030 (2011), http://stacks.iop.org/0029-5515/51/i=6/a=063030.
[54]H. Müller, T. Lunt, W. Suttrop, T. Eich, R. Fischer, J. Fuchs, A. Herrmann, M. Kočan, P. de Marné, and E. Wolfrum, J. Nucl. Mater. **438**, Supplement, S64 (2013); Proceedings of 20th International Conference on Plasma-Surface Interactions in Controlled Fusion Devices (PSI-20), Aachen (Germany), 20–25

This article is copyrighted as indicated in the article. Reuse of AIP content is subject to the terms at: http://scitation.aip.org/termsconditions. Downloaded to IP: 150.178.3.9 On: Tue, 06 May 2014 07:32:21

May, 2012, http://www.sciencedirect.com/science/article/pii/S0022311513000184.
[55]G. Ciaccio, O. Schmitz, M. Agostini, M. E. Puiatti, P. Scarin, G. Spizzo, N. Vianello, and R. B. White, in *Proc. 40th EPS Conference on Plasma Physics*, edited by V. Naulin, C. Angioni, M. Borghesi, S. Ratynskaia, S. Poedts, and T. Donné (European Physical Society (Petit Lancy), Helsinki, Finland, 2013), Vol. 37D, p. P1.107, http://ocs.ciemat.es/EPS2013PAP/pdf/P1.107.pdf.
[56]M. Barp, R. Cavazzana, G. Marchiori, A. Soppelsa, and L. Zanotto, Fusion Eng. Design **86**, 1000 (2011); Proceedings of the 26th Symposium of Fusion Technology (SOFT-26), Porto, Portugal 27 September–1 October 2010, http://www.sciencedirect.com/science/article/pii/S0920379611003218.
[57]J. Y. Hsu, V. S. Chan, R. W. Harvey, R. Prater, and S. K. Wong, Phys. Rev. Lett. **53**, 564 (1984), http://link.aps.org/doi/10.1103/PhysRevLett.53.564.

This article is copyrighted as indicated in the article. Reuse of AIP content is subject to the terms at: http://scitation.aip.org/termsconditions. Downloaded to IP: 150.178.3.9 On: Tue, 06 May 2014 07:32:21